Lattice Boltzmann approach to thermal transpiration

Victor Sofonea*

Center for Fundamental and Advanced Technical Research, Romanian Academy, Bd. Mihai Viteazul 24, RO – 300223 Timişoara, Romania

(Received 12 April 2006; revised manuscript received 14 September 2006; published 16 November 2006)

Diffuse reflection boundary conditions are introduced in a thermal lattice Boltzmann model to allow for variable fluid density and temperature along the walls. The capability of this model to capture the main characteristics of the thermal transpiration phenomenon in a box at nonvanishing Knudsen numbers is demonstrated. The thermal creep velocity is found to be proportional to the temperature gradient imposed at the wall, whereas the accuracy of the simulation results are found to be of first or second order, depending on the numerical scheme.

DOI: 10.1103/PhysRevE.74.056705 PACS number(s): 47.11.−j, 47.45.−n, 51.10.+y, 67.40.Hf

I. INTRODUCTION

Gas creeping *from cold toward hot* may start in a channel where a tangential temperature gradient $\partial T/\partial s$ is imposed along the walls [1]. This is the so-called transpiration phenomenon and is observed in rarefied gases when the Knudsen number $\mathrm{Kn}=\lambda/h$, expressed as the ratio between the mean free path λ and the characteristic size h of the channel, is no longer negligible. The creep velocity u_c is found to be proportional to $\partial T/\partial s$

$$u_c = \frac{3}{4}\frac{\mu R}{P}\frac{\partial T}{\partial s}. \tag{1}$$

Here, μ is the dynamic viscosity of the fluid, R is the ideal gas constant and P is the local pressure [1].

Because of their particulate nature, traditional tools used to simulate fluid physics at non-negligible values of the Knudsen number, like molecular dynamics (MD) or direct simulation Monte Carlo (DSMC), need huge memory and computing time that can easily exceed the capacity of today's supercomputers [2–5]. Lattice Boltzmann (LB) models use distribution functions instead of particles [6] and provide a mesoscopic level alternative to both particulate methods, as well as to standard techniques of computational fluid dynamics (CFD) derived from the principles of continuum media mechanics. The use of LB models to investigate flow phenomena at non-negligible Knudsen numbers has received considerable attention in recent time [7] due to increasing need for simulation of fluid flow at two extreme scales: high-altitude aerodynamics and micro- or nanosize devices known as microelectromechanical systems (MEMS). Unfortunately, the majority of LB applications developed up to date for non-negligible Knudsen number refer to the isothermal case. In this paper, we approach the thermal transpiration phenomenon using the two-dimensional LB model of Watari and Tsutahara [8], which allows us to investigate fluid flow with variable temperature.

*E-mail address: sofonea@acad-tim.tm.edu.ro

II. DESCRIPTION OF THE MODEL

The thermal LB model [8] uses 33 velocity vectors

$$\mathbf{e}_{00} = 0$$

$$\mathbf{e}_{ki} = \left[\cos\frac{\pi(i-1)}{4}, \quad \sin\frac{\pi(i-1)}{4}\right]c_k$$

$$k = 1, \ldots 4, \quad i = 1, \ldots 8. \tag{2}$$

The values of the speeds c_k $(k=1,\ldots 4)$

$$\{c_k\} = \{1.0, 1.92, 2.99, 4.49\} \tag{3}$$

were determined in [8] to ensure the stability of this model within the largest possible temperature range $(0.4 \le \theta \le 1.6)$. The corresponding distribution functions $f_{ki}=f_{ki}(\mathbf{x},t)$ evolve according to the LB equations

$$\partial_t f_{ki} + \mathbf{e}_{ki}\cdot\nabla f_{ki} = -\frac{1}{\tau}[f_{ki} - f_{ki}^{eq}] \tag{4}$$

and the local values of the fluid density $n=n(\mathbf{x},t)$, velocity $\mathbf{u}=\mathbf{u}(\mathbf{x},t)$, and temperature $\theta=\theta(\mathbf{x},t)$ are defined as follows:

$$n = f_{00} + \sum_{k=1}^{4}\sum_{i=1}^{8} f_{ki}, \tag{5}$$

$$n\mathbf{u} = \sum_{k=1}^{4}\sum_{i=1}^{8} f_{ki}\mathbf{e}_{ki}, \tag{6}$$

$$n\left(\theta + \frac{1}{2}u^2\right) = \sum_{k=1}^{4}\sum_{i=1}^{8}\frac{1}{2}f_{ki}c_k^2. \tag{7}$$

The density-dependent relaxation time $\tau=\Lambda/n\bar{c}$, where $\Lambda=1.0\times 10^6$ and

$$\bar{c} = \frac{\sum_{k=1}^{4} c_k \sum_{i=1}^{8} f_{ki}}{f_{00} + \sum_{k=1}^{4}\sum_{i=1}^{8} f_{ki}} \tag{8}$$

is the average speed of fluid particles, enables us to achieve various values of the local Knudsen number $\mathrm{Kn}=\Lambda/n$ [9]. The equilibrium distribution functions [8]

$$f_{ki}^{eq} = f_{ki}^{eq}(\mathbf{x},t) = nF_k s_{ki} \tag{9}$$

are expressed using the series expansion $s_{ki}=s_{ki}(\theta,\mathbf{u})$ up to fourth order with respect to the local fluid velocity $\mathbf{u}$, which has the Cartesian components u_α, $\alpha=1,2$ (summation over repeated Greek indices is understood),

$$s_{ki} = \left(1 - \frac{u^2}{2\theta} + \frac{u^4}{8\theta^2}\right) + \frac{1}{\theta}\left(1 - \frac{u^2}{2\theta}\right) e_{ki\xi}u_\xi + \frac{1}{2\theta^2} \times \left(1 - \frac{u^2}{2\theta}\right) e_{ki\xi}e_{ki\eta}u_\xi u_\eta + \frac{1}{6\theta^3} e_{ki\xi}e_{ki\eta}e_{ki\zeta}u_\xi u_\eta u_\zeta + \frac{1}{24\theta^4} e_{ki\xi}e_{ki\eta}e_{ki\zeta}e_{ki\chi}u_\xi u_\eta u_\zeta u_\chi. \tag{10}$$

The weight functions $F_k=F_k(\theta)$ that appear in Eq. (9) are given by

$$F_k = \frac{1}{c_k^2(c_k^2 - c_{\{k+1\}}^2)(c_k^2 - c_{\{k+2\}}^2)(c_k^2 - c_{\{k+3\}}^2)} \left[48\theta^4 - 6(c_{\{k+1\}}^2 + c_{\{k+2\}}^2 + c_{\{k+3\}}^2)\theta^3 + (c_{\{k+1\}}^2 c_{\{k+2\}}^2 + c_{\{k+2\}}^2 c_{\{k+3\}}^2 + c_{\{k+3\}}^2 c_{\{k+1\}}^2)\theta^2 - \frac{c_{\{k+1\}}^2 c_{\{k+2\}}^2 c_{\{k+3\}}^2 \theta}{4} \right]$$

$$F_0 = 1 - 8(F_1 + F_2 + F_3 + F_4), \tag{11}$$

where we used the notation $(l=1,2,3)$

$$\{k+l\} = \begin{cases} k+l, & k+l \le 4 \\ k+l-4, & k+l > 4. \end{cases} \tag{12}$$

We refer the reader to the literature for further details on the thermal LB model [8,9].

III. BOUNDARY CONDITIONS

Appropriate boundary conditions are introduced to allow the general case when the prescribed temperature may vary along the wall. These boundary conditions are derived using the concept of diffuse reflection, which dates back to the time of Maxwell and Smoluchowski [3,9–11]. For this purpose, the *thermalization process* is decoupled and the distribution functions whose velocities point normal to the wall mix separately from the distribution functions corresponding to velocities orientated along the diagonal of the square lattice. Unlike the procedure introduced in [9], this one allows also the fluid density to evolve freely along the walls.

For convenience, we restrict ourselves to the description of the diffuse reflection boundary conditions in the lattice nodes near the lower left corner of a box (Fig. 1). The mixing points (i.e., the black squares in Fig. 1) are located on the wall moving with velocity $\mathbf{u}_W$ and may have different temperatures $\theta_W^{j,l}$. In these points, the fluid density $\rho_W^{j,l}$ is allowed to evolve freely. Appropriate boundary conditions are needed to compute the values of the following distribution functions f_{ki}^{jl} defined in the ghost nodes (j,l) near the lower left corner in Fig. 1 $(k=1,\ldots 4)$:

$$f_{k8}^{0,2}, f_{k2}^{0,1}, f_{k1}^{0,1}, f_{k2}^{0,0}, f_{k3}^{1,0}, f_{k2}^{1,0}, f_{k4}^{2,0}. \tag{13}$$

Similar procedures may be used to compute the values of the distribution functions in the remaining ghost nodes outside the box.

The requirement that the distribution functions follow the Maxwellian distribution law at the mixing points on the left wall reads $(k=1,\ldots 4,\ l=1,2,\ldots)$

$$\frac{f_{k1}^{0,l} + f_{k1}^{1,l}}{F_k(\theta_W^{1/2,l}) s_{k1}(\theta_W^{1/2,l}, \mathbf{u}_W)} = 2\rho_W^{1/2,l} \tag{14a}$$

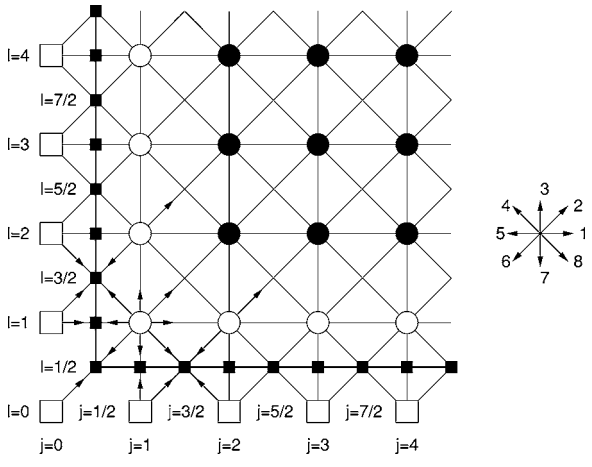

FIG. 1. Diffuse reflection boundary conditions near the lower left corner of a box: •=bulk nodes, ◦=boundary nodes, □=ghost nodes, ■=wall points where the distribution functions f_{ki}^{jl} follow the Maxwellian distribution law.

$$\frac{f_{k2}^{0,l}+f_{k2}^{1,l+1}}{F_k(\theta_W^{1/2,l+1/2})s_{k2}(\theta_W^{1/2,l+1/2},\mathbf{u}_W)}=\frac{f_{k8}^{0,l+1}+f_{k8}^{1,l}}{F_k(\theta_W^{1/2,l+1/2})s_{k8}(\theta_W^{1/2,l+1/2},\mathbf{u}_W)}=2\rho_W^{1/2,l+1/2}. \quad (14b)$$

Since $\theta>0$, one can easily see that the denominators in the equations above never vanish. Equations (14), together with the requirements that there is no mass flux perpendicular to the wall in the mixing nodes

$$\sum_{k=1}^{4} c_k f_{k5}^{1,l}=\sum_{k=1}^{4} c_k f_{k1}^{0,l} \quad (15a)$$

$$\sum_{k=1}^{4} c_k[f_{k4}^{1,l}+f_{k6}^{1,l+1}]=\sum_{k=1}^{4} c_k[f_{k2}^{0,l}+f_{k8}^{0,l+1}], \quad (15b)$$

may be solved to get the values of the distribution functions in the ghost nodes $(0,l)$ and $(0,l+1)$ after each time step. Similar equations may be introduced in order to compute the values of $f_{k3}^{j,0}$, $f_{k2}^{j,0}$, $f_{k4}^{j+1,0}$ $(k=1,\ldots 4, j=1,2,\ldots)$. The following relations will be used to compute the values of the distribution functions $f_{k2}^{0,0}$ $(k=1,\ldots 4)$:

$$\frac{f_{k2}^{0,0}+f_{k2}^{1,1}}{F_k(\theta_W^{1/2,1/2})s_{k2}(\theta_W^{1/2,1/2},\mathbf{u}_W)}=2\rho_W^{1/2,1/2}, \quad (16a)$$

$$\sum_{k=1}^{4} c_k f_{k6}^{1,1}=\sum_{k=1}^{4} c_k f_{k2}^{0,0}. \quad (16b)$$

Since the nondimensionalized speeds in the thermal LB model are no longer related to lattice spacing, as in standard LB models [6], finite difference schemes need to be used to evolve the distribution functions in each lattice nodes [8,9]. Besides the first order upwind scheme widely used to compute the gradient operator in the LB evolution equations [9], we considered also second order numerical schemes like the monitorized central difference (MCD) flux limiter [12] or the weighted essentially nonoscillatory (WENO) scheme [13]. These schemes were used to improve numerical accuracy in the bulk nodes (marked •) in Fig. 1. The first-order upwind scheme was always used to evolve the distribution functions in the boundary nodes (marked ◦) in Fig. 1, which are adjacent to the walls and subjected to the diffuse reflection boundary conditions introduced above.

IV. COMPUTER SIMULATION RESULTS

To investigate the capability of our improved boundary conditions to capture the thermal transpiration phenomenon, we considered the simplest case of a gas in a two-dimensional (2D) box at rest (Fig. 2). No external forces (such as gravity) are acting on the gas. For convenience, we set $L=2$ (in nondimensionalized units) and $h/L=0.1$. Wall temperatures are constant at the left (T_{left}) and right (T_{right}) ends of the box and change linearly along the horizontal walls, for $x\in[L/4,3L/4]$.

Computer simulations were done on a 200×20 lattice using the three numerical schemes mentioned previously

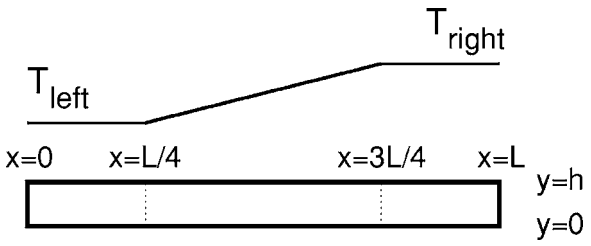

FIG. 2. Two-dimensional box used to simulate thermal transpiration. Temperature increases linearly from T_{left} to T_{right} along the horizontal walls (between $x=L/4$ to $x=3L/4$).

(first order upwind, MCD flux limiter and WENO). At $t=0$, the box was always filled with gas at rest, of temperature $T=(T_{\text{left}}+T_{\text{right}})/2=1.0$ and mean density $\bar{n}$ with 0.1% fluctuations. In all cases, we performed 500 000 iterations with time step $\delta t=10^{-4}$ to ensure the stationary flow state.

Figure 3 shows the stationary velocity field recovered using the WENO scheme, for $\bar{n}=10^8$ and the following values of the nondimensionalized wall temperatures: $T_{\text{left}}=0.90$, $T_{\text{right}}=1.10$. The formation of two vortices due to thermal transpiration is clearly seen. Because of the creep velocity $u_x=u_c>0$ near the walls, the fluid flows in the opposite direction in the center of the channel to balance the mass flow in the stationary state.

The MCD and WENO schemes, both of second order in the lattice spacing, give quite identical results, as seen in Fig. 4, which shows the transversal velocity profiles $u_x(x=L/2,y)$. When decreasing the mean gas density $\bar{n}$, the Knudsen number becomes noticeable, the thermal transpiration is enhanced and the magnitude of the fluid velocity in the middle of the box becomes larger in order to balance the mass flux due to the creep velocity near the walls.

When using the first-order upwind scheme in the bulk nodes of the 200×20 lattice, the mass flux in the center of the channel clearly exceeds the opposite flux near the walls [Fig. 5(a)]. This is due to the spurious velocity, which has the same sign as the density gradient [14]. The gas density is larger near the left wall of the box because its temperature is lower than the right one. The velocity profiles in Fig. 5 are

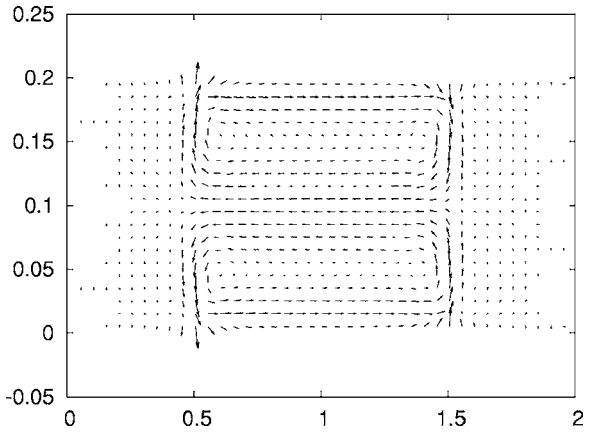

FIG. 3. Stationary velocity field due to thermal transpiration in a 2D box (200×20 nodes, $\bar{n}=10^8$, $T_{\text{left}}=0.90$, $T_{\text{right}}=1.10$), as recovered using the WENO scheme.

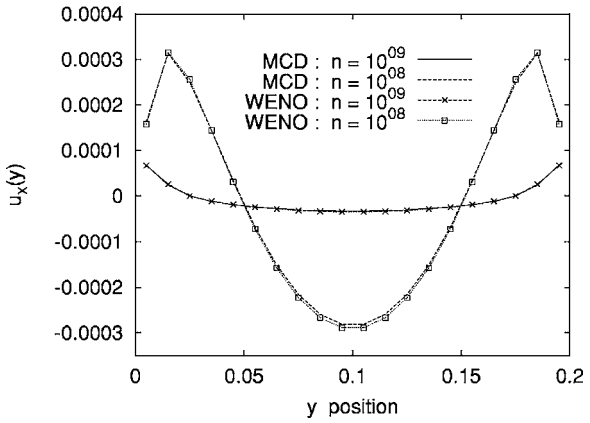

FIG. 4. Comparison of velocity profiles $u_x(y)$ at $x=L/2$ recovered on the 200×20 lattice using the MCD and WENO schemes, for two values of the mean fluid density $\bar{n}$.

the superposition of the velocity generated by the thermal transpiration and the spurious velocity, which plagues LB simulations. The spurious velocity may be significantly reduced when the number of lattice nodes per unit length is increased, or when using higher-order schemes [12]. Velocity profiles recovered with the first-order upwind scheme [Fig. 5(a)] strongly depend on the number of nodes N per unit length, which determines also the lattice spacing $\delta s=L/N$.

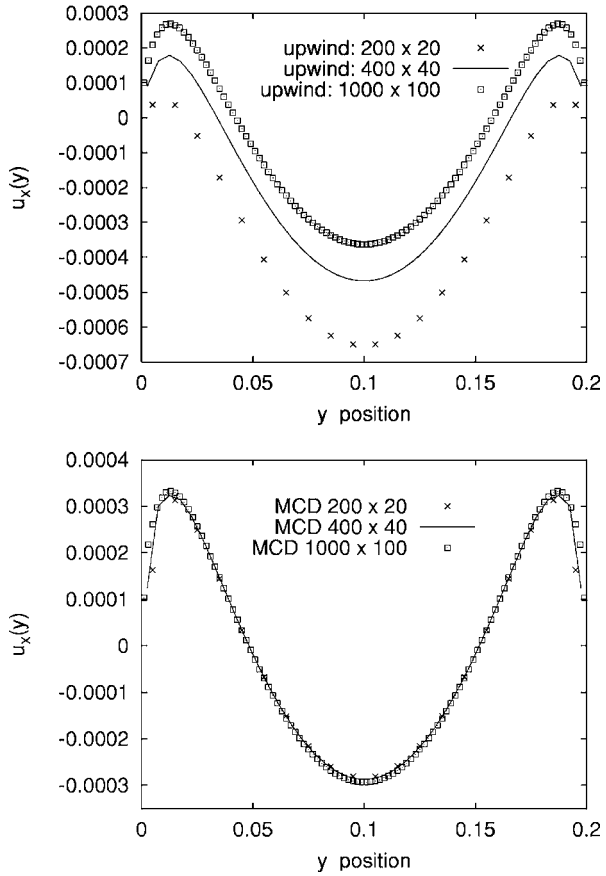

FIG. 5. Velocity profiles $u_x(y)$ at $x=L/2$ recovered with the upwind and MCD schemes on the 200×20, 400×40, and 1000×100 lattices ($\bar{n}=10^8$).

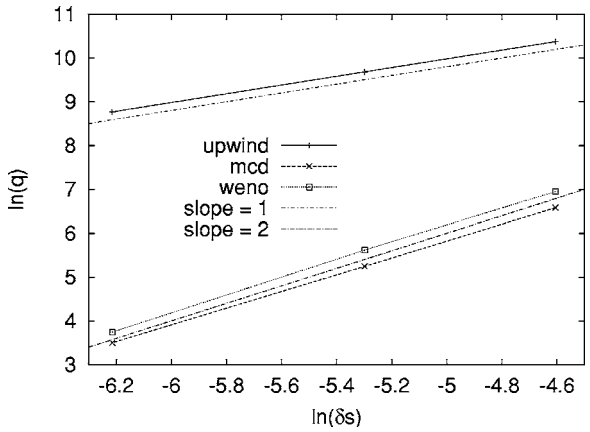

FIG. 6. Dependence of apparent mass flux q [Eq. (17)] vs lattice spacing δs, for various numerical schemes used in the lattice Boltzmann model.

The results recovered using the second-order schemes (MCD flux limiter and WENO) remain practically unchanged, except near the walls, as seen in Fig. 5(b) (this is not surprising since the diffuse reflection boundary conditions we use in our simulations were particularly designed for the first-order upwind scheme).

In the stationary regime, the total mass flux

$$q\left(x=\frac{L}{2}\right)=\frac{1}{h}\int_0^h \rho\left(x=\frac{L}{2},y\right)u_x\left(\frac{L}{2},y\right)dy \qquad (17)$$

should vanish. Because of numerical errors, we expect the apparent value of the mass flux q to exhibit a linear dependence on δs when using the first-order upwind scheme. In the case of flux limiter or WENO schemes, the dependence of the apparent mass flux q with respect to the lattice spacing is expected to be parabolic. Figure 6 shows the dependence $\ln(q)$ vs $\ln(\delta s)$ as recovered using the three numerical schemes mentioned above on the three lattices (200×20, 400×40, 1000×100). The results are in good agreement with our expectations.

The creep velocity extrapolated in the point $(x=1,y=0)$ of the bottom wall is found to be linearly dependent on the

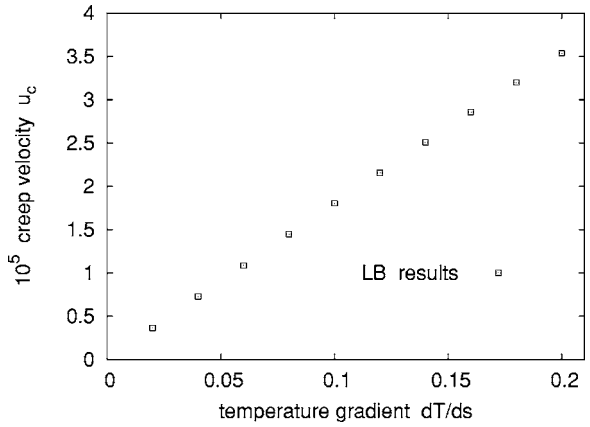

FIG. 7. Dependence of creep velocity u_c vs wall temperature gradient dT/ds ($\bar{n}=10^8$, MCD scheme, 400×40 nodes).

temperature gradient dT/ds (Fig. 7), as expected according to Eq. (1).

V. CONCLUSION

The diffuse reflection boundary conditions for the thermal finite difference lattice Boltzmann model with multiple speeds [8,9] were improved in this paper to allow the general case when the temperature and fluid density may change along the walls. These conditions account for the thermalization process where the distribution functions of the incoming particles are redistributed in the wall nodes to generate the corresponding values of the distribution functions of the outgoing (reflected) particles, which depend on the wall's temperature and velocity. The improved model was used to investigate the main characteristics of the thermal transpiration phenomenon, which occurs in a two-dimensional box when a tangential temperature gradient is imposed along the walls: vortex formation, velocity profile, and linear dependence of creep velocity vs wall temperature gradient. This demonstrates again the capability of the thermal LB model with diffuse reflection boundary conditions to capture flow phenomena at non-negligible Knudsen numbers. Because of their statistical character, feasibility, and noise reduction with respect to MD and DSMC models, we expect LB models to become a basic tool for the exploration, design, development, and optimization of micro- and nanoscale technologies.

ACKNOWLEDGMENTS

This work was supported by U.S. Air Force European Office of Aerospace Research and Development (EOARD) Grant No. FA8655--05--M--4008 and Romanian National Authority for Scientific Research (ANCS) Grant No. CEEX 11/2005. Computer simulations were done using the Portable Extensible Toolkit for Scientific Computation (PETSc) developed at Argonne National Laboratory, Argonne, Illinois [15].

[1] G. E. Karniadakis and A. Beskok, *Micro Flows: Fundamentals and Simulation* (Springer-Verlag, Berlin, 2002); *Microfluidique*, edited by S. Colin (Hermes Science, Paris, 2004); C. Shen, *Rarefied Gas Dynamics: Fundamentals, Simulations and Micro Flows* (Springer-Verlag, Berlin, 2005); P. Tabeling, *Introduction to Microfluidics* (Oxford University Press, London, 2005).

[2] E. S. Oran, C. K. Oh, and B. Z. Cybyk, Annu. Rev. Fluid Mech. **30**, 403 (1998).

[3] M. Gad-el-Haq, J. Fluids Eng. **121**, 5 (1999).

[4] J. M. Reese, M. A. Gallis, and D. A. Lockerby, Philos. Trans. R. Soc. London, Ser. A **361**, 2967 (2003).

[5] *MEMS: Introduction and Fundamentals*, edited by M. Gad-el-Haq (CRC Press, Boca Raton, 2005).

[6] D. H. Rothman and S. Zaleski, *Lattice Gas Cellular Automata: Simple Models of Complex Hydrodynamics* (Cambridge University Press, Cambridge, England, 1997); B. Chopard and M. Droz, *Cellular Automata Modeling of Physical Systems* (Cambridge University Press, Cambridge, England, 1998); D. A. Wolf-Gladrow, *Lattice Gas Cellular Automata and Lattice Boltzmann Models* (Springer-Verlag, Berlin, 2000); S. Succi, *The Lattice Boltzmann Equation for Fluid Dynamics and Beyond* (Clarendon Press, Oxford, 2001).

[7] X. Nie, G. D. Doolen, and S. Chen, J. Stat. Phys. **107**, 279 (2002); C. Lim, C. Shu, X. Niu, and Y. Chew, Phys. Fluids **14**, 2299 (2002); B. Li and D. Kwok, Phys. Rev. Lett. **90**, 124502 (2003); X. D. Niu, C. Shu, and Y. T. Chew, Europhys. Lett. **67**, 600 (2004); F. Toschi and S. Succi, *ibid.* **69**, 549 (2005); T. Lee and C. L. Lin, Phys. Rev. E **71**, 046706 (2005); Y. Zhang, R. Qin, and D. R. Emerson, *ibid.* **71**, 047702 (2005); M. Sbragaglia and S. Succi, Phys. Fluids **17**, 093602 (2005).

[8] M. Watari and M. Tsutahara, Phys. Rev. E **67**, 036306 (2003).

[9] V. Sofonea and R. F. Sekerka, Phys. Rev. E **71**, 066709 (2005).

[10] J. C. Maxwell, Philos. Trans. R. Soc. London **170**, 231 (1879); M. Smoluchowski, Ann. Phys. Chem. **64**, 101 (1898); W. G. Vincenti and C. H. Kruger, *Introduction to Physical Gas Dynamics* (Wiley, New York, 1965); C. Cercignani, *Rarefied Gas Dynamics: From Basic Concepts to Actual Calculations* (Cambridge University Press, Cambridge, England, 2000).

[11] S. Ansumali and I. V. Karlin, Phys. Rev. E **66**, 026311 (2002).

[12] A. Cristea and V. Sofonea, Cent. Eur. J. Phys. **2**, 382 (2004); V. Sofonea, A. Lamura, G. Gonnella, and A. Cristea, Phys. Rev. E **70**, 046702 (2004); V. Sofonea and R. F. Sekerka, Int. J. Mod. Phys. C **16**, 1075 (2005).

[13] C. W. Shu, in *High-Order Methods for Computational Physics*, edited by T. J. Barth and H. Deconinck (Springer-Verlag, Berlin, 1999).

[14] A. Cristea and V. Sofonea, Int. J. Mod. Phys. C **14**, 1251 (2003).

[15] S. Balay, K. Buschelman, V. Eijkhout, W. Gropp, D. Kaushik, M. Knepley, L. C. McInnes, B. Smith, and H. Zhang, Tech. Rep. No. ANL-95/11- Revision 2.2.1, Argonne National Laboratory, http://www.mcs.anl.gov/petsc (2004).